Precipitation Reactions and Strengthening Behavior in 18 Wt Pct Nickel Maraging Steels

VIJAY K. VASUDEVAN, SUNG J. KIM, and C. MARVIN WAYMAN

The crystallography, structure, and composition of the strengthening precipitates in maraging steels C-250 and T-250 have been studied utilizing analytical electron microscopy and computer-simulated electron diffraction patterns. The kinetics of precipitation were studied by electrical resistivity and microhardness measurements and could be described adequately by the Johnson-Mehl-Avarami equation, with precipitate nucleation occurring on dislocations and growth proceeding by a mechanism in which the dislocations serve as collector lines for solute from the matrix along which pipe diffusion occurs. The strengthening of the Co-free, higher Ti T-250 steel is caused by a refined distribution of Ni_3Ti precipitates. High strength is maintained at longer times from the combined effect of a high resistance of these precipitates to coarsening and a small volume fraction of reverted austenite. In the case of the Co-containing, lower Ti C-250 steel, strengthening results from the combined presence of Ni_3Ti (initially) and Fe_2Mo precipitates (at longer times). Loss of strength at longer times is associated, in part, with overaging and mainly from the larger volume fraction of reverted austenite. The resistance to austenite reversion is dependent on the manner in which the relative nickel content of the martensite matrix is affected by the precipitating phases, and the difference in the reversion tendency between the two steels can be explained on this basis.

I. INTRODUCTION

MARAGING steels are low-carbon martensitic steels developed in the 1960s for applications requiring ultra-high strength combined with good fracture toughness.[1] These steels usually contain about 18 wt pct Ni, together with substitutional elements such as Co, Mo, and Ti. The initial steels developed, referred to as "C-grade," contained about 8 to 9 wt pct Co, 4 to 5 wt pct Mo, and small amounts of Ti. More recently, "T-grade" steels free of Co but containing higher amounts of Ti have been developed. Typically, the steels are solution treated in the fully austenite region (>800 °C), quenched to produce a completely martensitic matrix, and subsequently aged at intermediate temperatures (400 °C to 500 °C) to cause precipitation hardening. Substantial strengthening, often in excess of 300 ksi, can be achieved in this way. The high strength, combined with good fracture toughness, is obtained by the precipitation of intermetallic phases in the soft martensite matrix. Numerous studies have been carried out to determine the nature of the maraging precipitates. However, there exists a considerable diversity of opinion on the nature of the strengthening precipitates, particularly in the C-grade steels. For instance, in C-grade steels of similar composition, several different kinds of precipitates, such as Ni_3Mo,[2–5] Ni_3Ti,[4,5,6] Fe_2Mo,[6,7,8] FeTi,[2] and Fe_2Ti,[3] have been reported. Often more than one kind of precipitate has been reported.[2–7] In the T-grade steels, Ni_3Ti has been reported to be the dominant precipitate.[9,10] This study was undertaken to determine the crystallography, structure, and composition of the strengthening precipitates in two commercial grades of maraging steels, designated C-250 and T-250. The results of electrical resistivity, microhardness, analytical electron microscopy, and computer-simulated electron diffraction patterns are presented and discussed.

II. EXPERIMENTAL METHODS

Maraging steel grades C-250 and T-250 in ingot form were obtained from commercial sources. The alloy compositions are shown in Table I. The principal difference in the composition of the two steels is in the amounts of Co, Ti, and Mo. The C-grade contains about 8 wt pct Co and 0.46 wt pct Ti, whereas the T-grade is free of Co but contains about 1.4 wt pct Ti. The Mo content is about 5 wt pct in the former and 3 wt pct in the latter.

The alloy ingots were sectioned and cold swagged, with intermediate anneals at 900 °C, to rods about 3 mm in diameter. Cut rods were sealed in quartz under vacuum, solution treated at 816 °C (1500 °F) for 6 hours, and then water quenched to produce a completely martensitic structure. Cut samples from the solution-treated rods were encapsulated in quartz under vacuum, aged at 427 °C (800 °F), 482 °C (900 °F), and 538 °C (1000 °F) for times ranging from 0.017 to 100 hours, and then water quenched to arrest further transformation.

Manual measurements of electrical resistivity were made by mechanically placing the heat-treated rods across a pair of calibrated knife edges and connecting the ends to a precisely controlled current source in series with a calibrated resistor. With a controlled current of 1.5 A passing, the voltage drop across the knife edges was measured and the resistivity calculated using the standard expression relating the resistivity to current, voltage, and specimen dimensions.

VIJAY K. VASUDEVAN, formerly with the University of Illinois, is Assistant Professor, Department of Materials Science and Engineering, University of Cincinnati, Cincinnati, OH 45221-0012. SUNG J. KIM, formerly with the University of Illinois, is Senior Engineer with the Korea Institute of Machinery and Metals, Kyungnam, Republic of Korea. C. MARVIN WAYMAN, Professor, is with the Department of Materials Science and Engineering, University of Illinois, Urbana, IL 61801.

Manuscript submitted July 3, 1989.

Table I. Chemical Composition of Maraging Steels (in Weight Percent)

Element	Steel	
	C-250	T-250
C	0.015	0.013
Ni	18.36	18.36
Mo	4.75	3.02
Co	8.18	0.11
Ti	0.46	1.34
Al	0.12	0.11
Fe	bal.	bal.

Microhardness measurements were made on mounted and polished samples in a TUKON* tester using a 1-kg load. A minimum of five readings was taken and the average calculated.

*TUKON is a trademark of Wilson Instruments, Bridgeport, CT.

Disks for transmission electron microscopy (TEM) were sliced from the heat-treated rods, chemically thinned to a thickness of about 0.025 mm, and then electropolished in a twin-jet thinning apparatus using a solution consisting of 5 pct perchloric acid and 95 pct glacial acetic acid with a voltage of 30 to 40 V, a current of 50 to 70 mA, and a temperature of 25 °C. Observations of the foils were carried out in a Hitachi H-800 electron microscope operated at 200 keV. Energy dispersive X-ray (EDX) microanalysis was conducted at 100 keV in a Vacuum Generators HB5 scanning transmission electron microscope equipped with a field emission gun. The chemical composition of the precipitates was determined using the standard ratio method.[11] The proportionality constant relating the concentration ratios of different elements to the corresponding intensity ratios was determined using thin film standards of the two steels in the solution-treated condition. To minimize contributions to the intensity spectrum from the underlying matrix, particles located at the edge of the holes in the thin foils were analyzed.

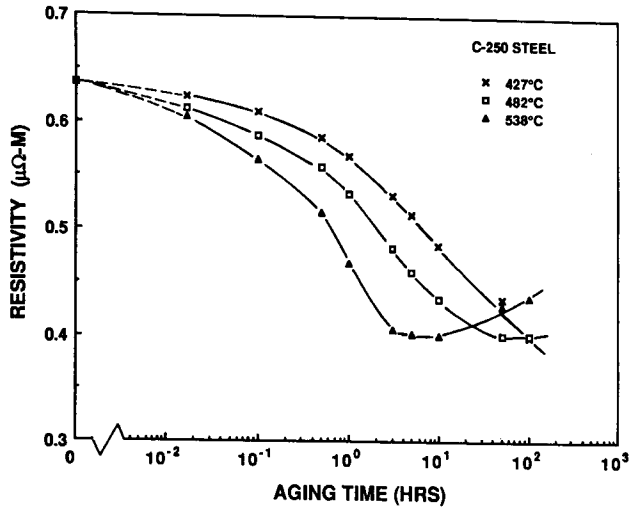

(*a*)

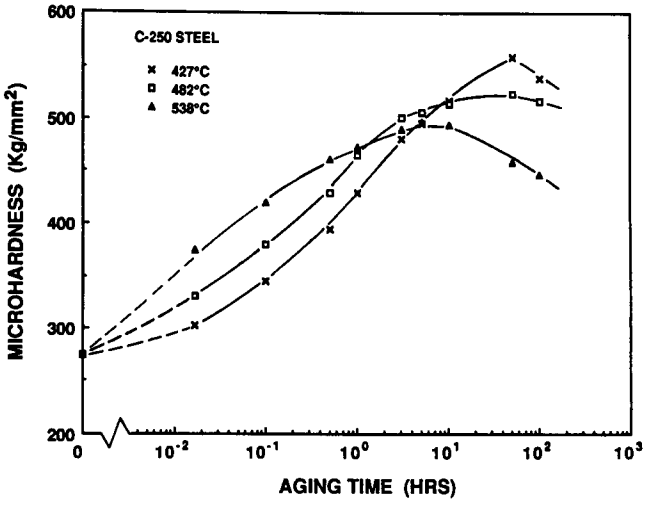

(*b*)

Fig. 1—Variation of (*a*) electrical resistivity and (*b*) microhardness of C-250 steel with aging time at various indicated temperatures.

III. RESULTS

A. *Electrical Resistivity and Microhardness*

The results of the variation of electrical resistivity and microhardness as a function of aging temperature and time are shown in Figures 1(a) and (b) and 2(a) and (b) for the C-250 and T-250 steels, respectively. The resistivity curves (Figures 1(a) and 2(a)) have three general characteristic features: (1) a small decrease at short times, (2) a large decrease at intermediate times, particularly in the C-grade steel, and (3) a leveling off at long aging times, followed by a final increase at higher temperatures, especially in the C-grade steel. These features are in general agreement with the report of Peters and Cupp.[12]

The small decrease in resistivity in stage 1 occurs within 0.1 hour and is accompanied by a modest increase in hardness. A small contribution to this decrease probably comes from recovery in the martensite matrix, whereas a major contribution is associated with accumulation of solute atoms on dislocations in the martensite matrix. The large decrease in resistivity in stage 2 is accompanied by a rapid increase in hardness and is associated with precipitation from solid solution. The resistivity minimum coincides with the peak hardness; the subsequent increase in resistivity at the higher temperatures in the C-grade steel is associated with reversion to austenite,[12] and lowering the temperature is more effective in suppressing austenite reversion than is the precipitation reaction.

The hardness responses of the two steels are generally similar (Figures 1(b) and 2(b)); only the peak hardness and subsequent decrease occur at shorter times at all aging temperatures in the T-250 steel. For example, the peak hardness occurs at 5, 50, and 50 hours at 538 °C, 482 °C, and 427 °C, respectively, in the C-250 steel compared to 2, 10, and 10 hours at the same temperatures in the T-250 steel. On the other hand, the resistivity behaviors show several significant differences. First, the solution-treated resistivity value of the C-250 steel (0.64 $\mu\Omega \cdot m$) is higher than that of the T-250 steel (0.57 $\mu\Omega \cdot m$). By means of a simple analysis, this difference can be related

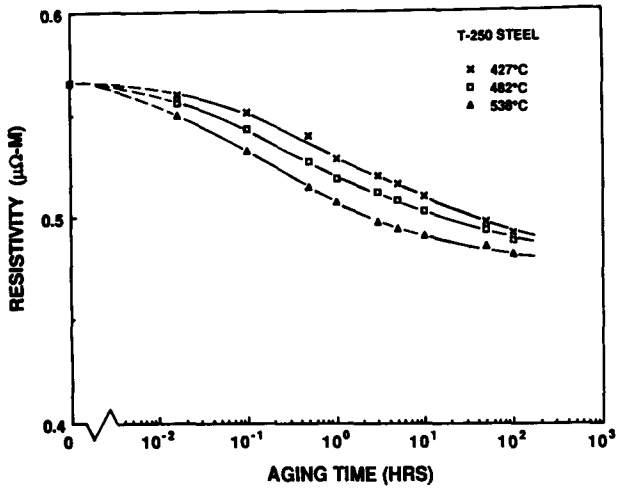

(*a*)

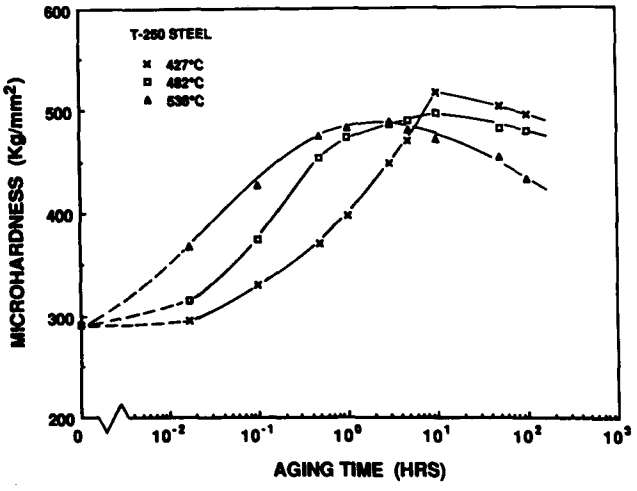

(*b*)

Fig. 2—Variation of (*a*) electrical resistivity and (*b*) microhardness of T-250 steel with aging time at various indicated temperatures.

to the relative contributions of Mo, Co, and Ti to the resistivity. A second feature of significance concerns the relative difference in the resistivity values of the solution-treated condition and that following aging. For example, within 3 hours, the resistivity of the C-250 steel decreases by 24 pct compared to 10 pct in the T-250 steel; the difference at the resistivity minimum is 40 pct compared to 15 pct. As shown later, this difference is associated with the additional precipitation of Fe_2Mo in the C-250 steel. A third feature is associated with the resistivity upturn at longer times. The T-250 steel does not show this feature, thus indicating that it is more resistant to austenite reversion compared to the C-250 steel.

The shape of the resistivity curves suggests that the kinetics of precipitation can be represented by the Johnson-Mehl-Avarami equation:

$$f = 1 - \exp(-kt^n) \qquad [1]$$

where f is the fraction transformed, t is the aging time, and k and n are constants for a given temperature.[13] The fraction transformed can be taken to be proportional to the resistivity change as follows:

$$f = (\rho_0 - \rho_t)/(\rho_0 - \rho_f) \qquad [2]$$

where ρ_0, ρ_f, and ρ_t represent the initial, final, and at time t resistivities. Combining Eqs. [1] and [2] and taking logs yields

$$\log\log[(\rho_0 - \rho_f)/(\rho_t - \rho_f)] = n\log t + \log k - \log 2.303 \qquad [3]$$

Thus, a plot of $\log\log[(\rho_0 - \rho_f)/(\rho_t - \rho_f)]$ against $\log t$ should yield a straight line of slope n. Equation [3] contains three unknowns, n, k, and ρ_f. The final resistivity, ρ_f, could not be determined experimentally due to the occurrence of austenite reversion. Therefore, to determine this value, the number of unknowns in Eq. [3] was reduced, and a set of simultaneous equations based on ρ_0, ρ_t, ρ_f, and t was developed. The values of ρ_f were then obtained numerically by using the known values of ρ_0 and ρ_t for t in the range of 1 to 50 hours. These values, which are dependent on composition and therefore on temperature, were 0.316, 0.351, and 0.366 $\mu\Omega \cdot$ m at 427 °C, 482 °C, and 538 °C, respectively, in the C-250 steel, and 0.45, 0.46, and 0.47 $\mu\Omega \cdot$ m at the same temperatures in the T-250 steel. Values of $\log\log[(\rho_0 - \rho_f)/(\rho_t - \rho_f)]$ thus obtained are shown plotted as a function of aging time in Figures 3(a) and (b) for the C-250 and T-250 steels, respectively, from which it can be seen that straight lines are obtained at each of the temperatures. The Avarami exponent, n, obtained from the slopes of these lines is 0.39, 0.39, and 0.45 at 427 °C, 482 °C, and 538 °C, respectively, in the C-250 steel; the values in the T-250 steel are much lower, being 0.20, 0.20, and 0.21, respectively, at the aforementioned temperatures.

The activation energy for precipitation was determined from the slope of the straight line obtained by plotting values of the log of the time required to attain a particular fraction transformed ($\log t_f$) against the reciprocal of the temperature ($1/T$ in K^{-1}). A plot of $\log t_f$ at $f = 50$ pct against $1/T$ is shown in Figure 4 for the two steels, from which the activation energy for both steels is obtained as 130 kJ/mole (31 kcal/mole). In both steels, this energy was found to vary from 101 kJ/mole (24 kcal/mole) at $f = 25$ pct to 181 kJ/mole (43 kcal/mole) at $f = 75$ pct.

B. *Electron Microscopy*

In the following, the subscript "M" is used to denote indices of directions and planes relative to the body-centered cubic (bcc) martensite. The solution-treated microstructure of both alloys consisted entirely of lath martensite with a high density of dislocations, as reported elsewhere.[14] The lattice parameter was determined by electron diffraction to be 0.288 nm. The habit plane of the laths was confirmed to be the $\{011\}_M$ plane, with the associated $\langle 111\rangle_M$ direction parallel to the long axis of the laths,[14] as reported by others.[1] Adjacent laths were observed to sometimes bear a twin relationship. The T-grade also showed some evidence of microtwins within individual laths.

The microstructural changes during aging at 482 °C

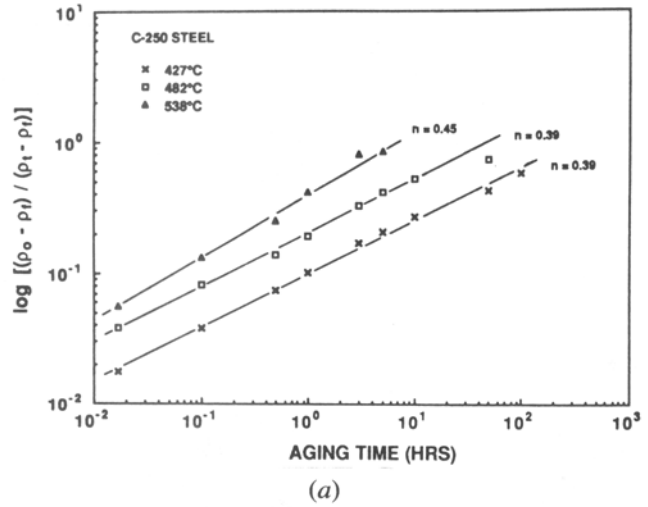

(a)

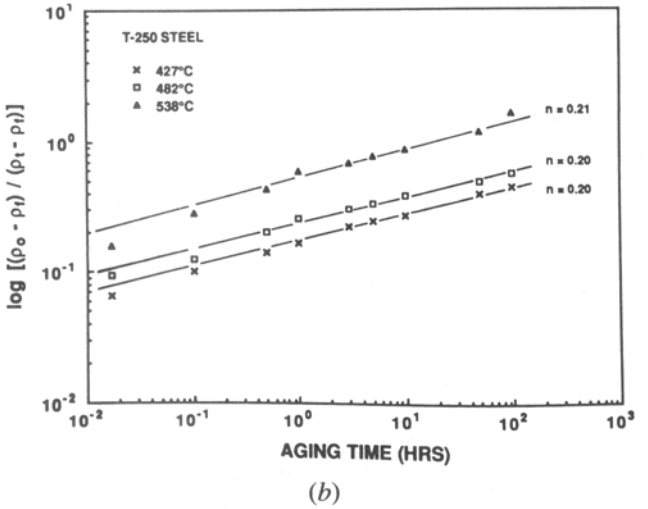

(b)

Fig. 3—Plot of log log $[(\rho_0 - \rho_f)/(\rho_t - \rho_f)]$ against aging time for (*a*) C-250 steel and (*b*) T-250 steel.

and 538 °C are described in the following. The aging behavior at 427 °C, in terms of the nature of the precipitates, was largely similar to that at 482 °C and is therefore not included. For the sake of convenience, the results of the T-grade steel are presented first.

1. *T-250 steel*

The microstructural changes that occur at 482 °C are described first. Electron diffraction patterns taken from samples aged for times up to 1 hour showed pronounced streaking extending through the martensite matrix spots, indicative of preprecipitation phenomena. Examination of diffraction patterns at a number of orientations revealed that the streaks were formed when the Ewald sphere intersects planar regions of diffuse scattering in reciprocal space normal to the $\langle 111 \rangle_M$ directions, which ultimately become the long axis of the precipitates. At 1 hour, weak precipitate spots appeared at locations where streaks intersected, and the spots themselves were streaked. A bright-field (BF) micrograph corresponding to this treatment (Figure 5) shows a very refined distribution of precipitates which appear to have nucleated on dislocations and lath boundaries. On further aging to

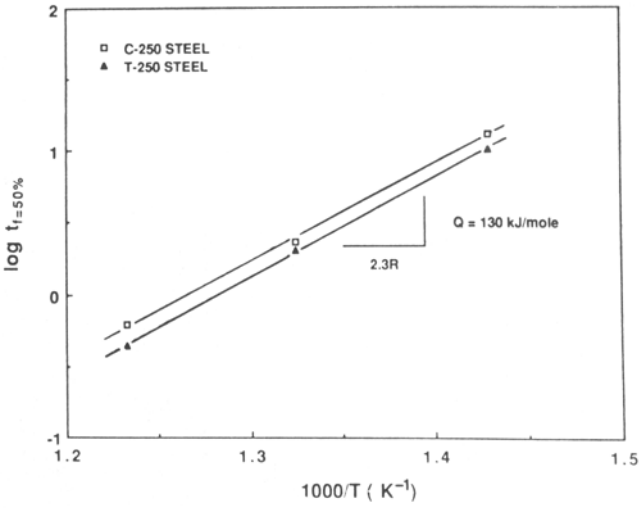

Fig. 4—Plot of log $t_{f=50\,pct}$ against $1/T$.

3 hours, the precipitate spots increased in intensity, and dark-field (DF) micrographs taken from the precipitate spots revealed thin, needlelike precipitates 4.5-nm wide and 25-nm long.[14] Thus, the streaking of the precipitate spots in the early stages can be attributed to the thinness of the precipitates.

The diffraction patterns obtained from samples aged for longer times (50 hours) (Figures 6(a) and (d)) are essentially similar to those obtained at shorter times, with one important difference. The precipitate spots are strong enough to permit unambiguous determination of their nature. Since the diffraction patterns are quite complex, computer simulations were used to aid in the interpretation. Based on measured interplanar spacings of different precipitate reflections and computer simulations, the diffraction patterns can be interpreted on the basis of precipitation of the hexagonal η-Ni_3Ti phase with $a = 0.5101$ nm and $c = 0.8307$ nm.[15,16] The measured *d*-spacings and those calculated for this phase are in

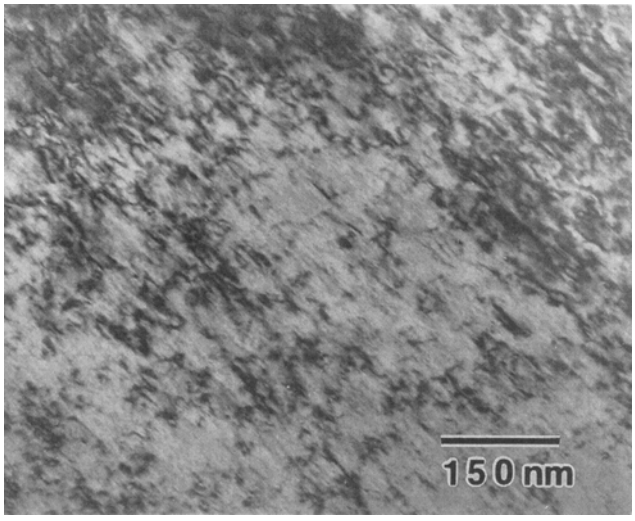

Fig. 5—T-250 steel aged at 482 °C for 1 h: BF micrograph showing precipitate nucleation on dislocations and martensite lath boundaries.

Table II. *d*-Spacings of Ni_3Ti

hkl	Measured	Calculated
$20\bar{2}0$	2.205	2.21
$20\bar{2}1$	2.134	2.135
0004	2.07	2.08
$20\bar{2}2$	1.96	1.95
$20\bar{2}3$	1.72	1.73
$12\bar{3}2$	1.54	1.55
$20\bar{2}5$	—	1.33
$22\bar{4}0$	1.28	1.27
$20\bar{2}6$	—	1.17
$40\bar{4}0$	1.10	1.10
$40\bar{4}1$	—	1.095
$22\bar{4}4$	1.085	1.087
$40\bar{4}2$	—	1.07
$40\bar{4}3$	—	1.03

excellent agreement, as shown in Table II. The orientation relationship observed between martensite and η-Ni_3Ti is

$$(011)_M//(0001)_\eta$$

$$[1\bar{1}1]_M//[11\bar{2}0]_\eta$$

This orientation relationship gives rise to 12 possible variants of precipitates shown listed in Table III.

The $[011]_M$ selected area diffraction (SAD) pattern taken from a sample aged for 50 hours is shown in Figure 6(a). The corresponding computer-simulated pattern, including matrix and precipitate spots, and both precipitate and double diffraction spots of the precipitate spots with each of the strong matrix spots are shown in Figures 6(b) and (c), respectively. In these patterns, the large open circles denote the matrix martensite spots; the small, filled circles denote precipitate spots; and the small, filled squares refer to double diffraction spots. Spots from two variants of precipitates, numbers 1 and 2 identified in Figure 6(b) and in Table III, are present. This pattern corresponds to the [0001] pattern of Ni_3Ti, and the $(22\bar{4}0)$ spots from variants 1 and 2 lie along the two associated $\langle 222\rangle_M$ directions. After including double diffraction, it can be seen that this pattern is in exact agreement with the experimental pattern. Generally, the $\{20\bar{2}0\}$ spots were very weak and often not present. Also, one of these spots from each variant practically coincides with the strong $(0\bar{1}1)_M$ spot and is therefore not visible in the simulation. Another feature is concerned with the presence of weak reflections in Figure 6(a). Since these reflections were also weakly present in solution-treated samples and appeared to persist following aging, they probably originate from a surface oxide film. Additional confirmation for this is provided by the fact that the locations of these reflections are identical to those reported for surface oxides of type R_3O_4 in ferritic steels.[17] The [113] SAD pattern taken from the same sample is shown in Figure 6(d); the corresponding computer-simulated patterns, with and without double diffraction, are shown in Figures 6(e) and (f), respectively. In this case, spots from eight variants of precipitates, numbers 1, 2, and 5 through 10 are present, and once again, after including double diffraction, exact agreement is obtained with the experimental pattern. Selected area diffraction patterns at other orientations could also be similarly simulated.

Table III. The Twelve Possible Variants of η-Ni_3Ti Relative to Martensite

Variant	Martensite	η-Ni_3Ti
1	$(011)\ [1\bar{1}1]$	$(0001)\ [11\bar{2}0]$
2	$(011)\ [\bar{1}\bar{1}1]$	$(0001)\ [11\bar{2}0]$
3	$(0\bar{1}1)\ [111]$	$(0001)\ [11\bar{2}0]$
4	$(0\bar{1}1)\ [\bar{1}11]$	$(0001)\ [11\bar{2}0]$
5	$(110)\ [\bar{1}11]$	$(0001)\ [11\bar{2}0]$
6	$(110)\ [\bar{1}\bar{1}\bar{1}]$	$(0001)\ [11\bar{2}0]$
7	$(\bar{1}10)\ [111]$	$(0001)\ [11\bar{2}0]$
8	$(\bar{1}10)\ [\bar{1}\bar{1}1]$	$(0001)\ [11\bar{2}0]$
9	$(101)\ [\bar{1}11]$	$(0001)\ [11\bar{2}0]$
10	$(101)\ [\bar{1}\bar{1}1]$	$(0001)\ [11\bar{2}0]$
11	$(\bar{1}01)\ [111]$	$(0001)\ [11\bar{2}0]$
12	$(\bar{1}01)\ [\bar{1}\bar{1}\bar{1}]$	$(0001)\ [11\bar{2}0]$

A BF micrograph of the same sample is shown in Figure 7(a). A DF micrograph (Figure 7(b)) taken from the $(22\bar{4}0)$ Ni_3Ti spot, indicated by the arrow in the corresponding $[112]_M$ SAD pattern in Figure 7(c), reveals that the precipitates are actually rod-shaped, 8 nm in diameter, and 42-nm long. The rod shape was confirmed by tilting experiments and observing the precipitates edge-on. A remarkable resistance to coarsening is evident. The habit plane and long axis of the precipitates correspond to the close-packed planes and close-packed directions of the bcc martensite and hexagonal Ni_3Ti described by the orientation relationship. Another feature observed in diffraction patterns, both at short times and somewhat more clearly at longer times, was the presence of weak spots at the $\{100\}_M$ locations. A typical example is shown in the $[001]_M$ SAD pattern in Figure 7(d). These spots have been attributed to either martensite-martensite double diffraction,[5] which is erroneous, or B2-type ordering in the martensite matrix,[6] for which positive confirmation could not be obtained, since the spot locations also correspond to the {110} reflections from surface Fe_3O_4.[17,18]

There is also evidence for the presence of reverted austenite, appearing as coarse, patchy regions at martensite lath boundaries (Figures 7(a) and (b)). The lattice parameter of austenite was determined by electron diffraction to be 0.36 nm, and the orientation relationship between martensite and austenite is given by the parallelism between the close-packed planes and directions in these structures, *i.e.*, the Kurdjumov-Sachs relationship. Moreover, the *d*-spacings of the {220} reflections of the austenite are practically identical to those of the $\{22\bar{4}0\}$ reflections of the hexagonal Ni_3Ti. Consequently, these spots virtually coincide in the diffraction patterns, and $[011]_M$ diffraction patterns with reverted austenite and Ni_3Ti (excluding the $\{20\bar{2}0\}$ reflections) appear identical. Better discrimination of the presence of reverted austenite, however, results by examining diffraction patterns at other orientations, particularly the $[111]_M$ orientation, where the austenite spots are clearly visible, whereas the {0004} Ni_3Ti spots coincide with the strong $\{011\}_M$ spots and are effectively masked.

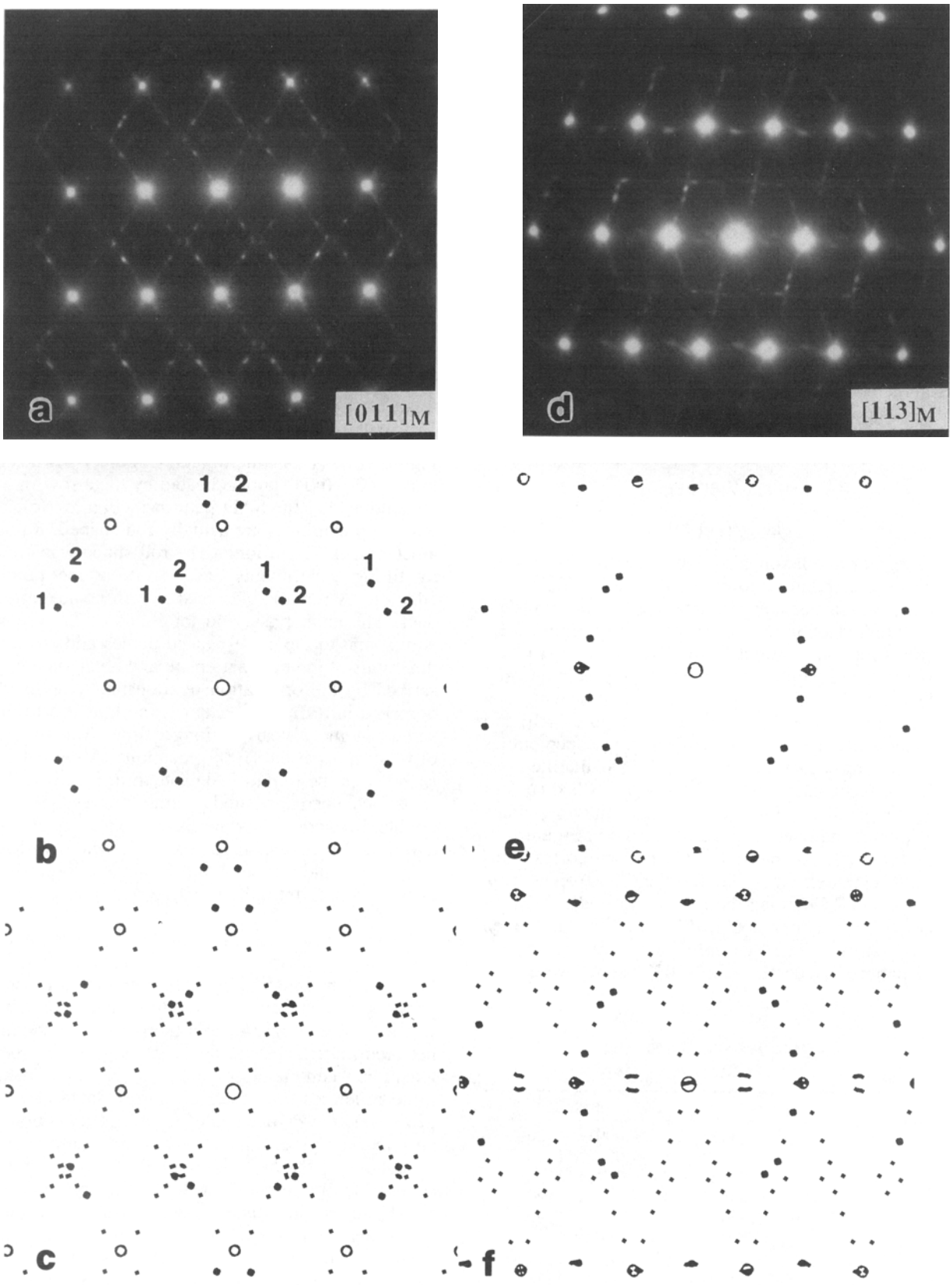

Fig. 6—T-250 steel aged at 482 °C for 50 h: (*a*) $[011]_M$ SAD pattern; (*b*) and (*c*) computer-simulated $[011]_M$ patterns; (*d*) $[113]_M$ SAD pattern; and (*e*) and (*f*) computer-simulated $[113]_M$ patterns. The large open circles denote martensite spots; the small, filled circles denote Ni_3Ti precipitate spots; and the small, filled squares refer to double diffraction spots (see Section III–B–1 for details).

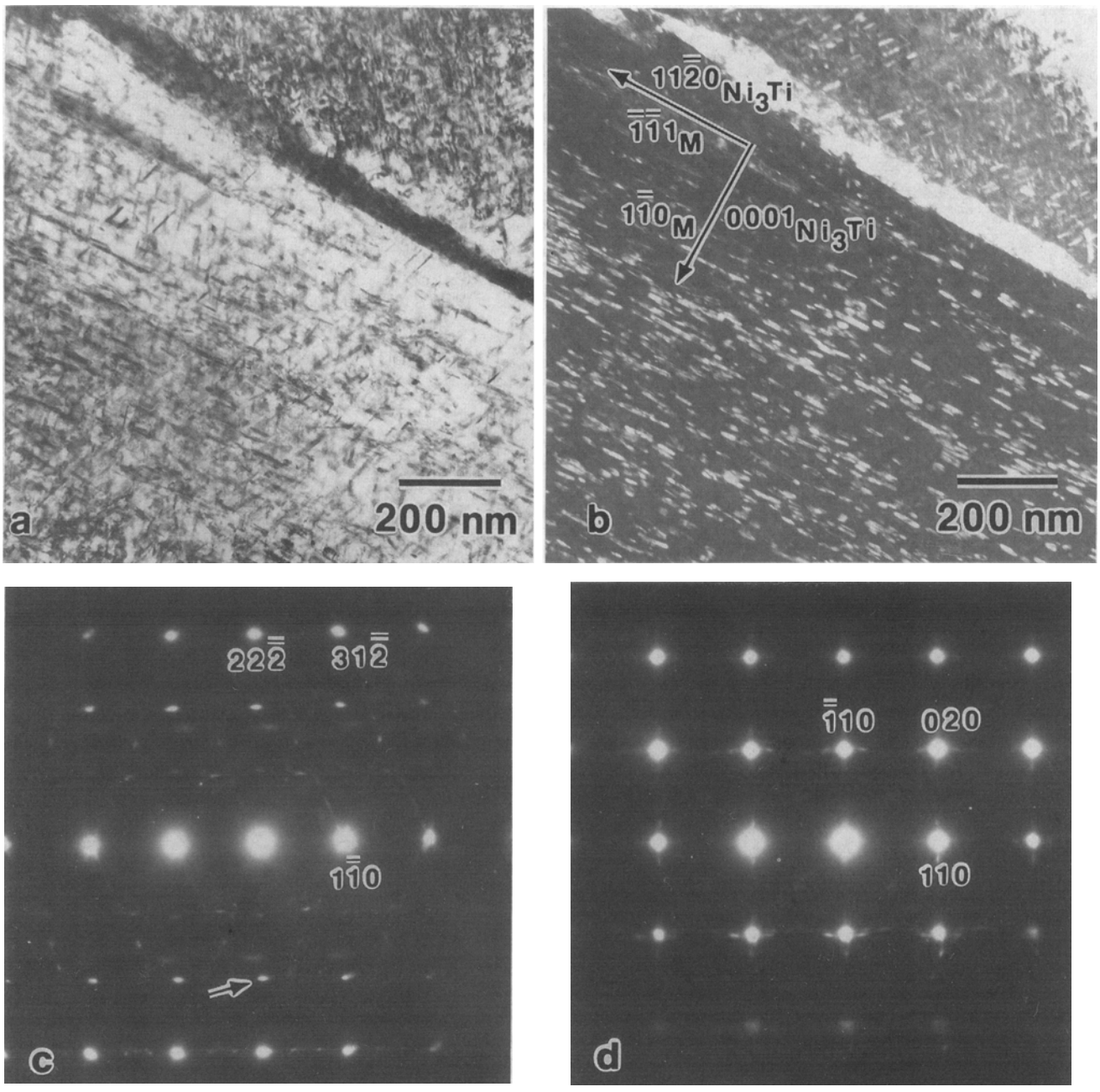

Fig. 7—T-250 steel aged at 482 °C for 50 h: (*a*) BF micrograph; (*b*) DF micrograph taken from the $(22\bar{4}0)$ Ni_3Ti spot indicated by the arrow in the $[112]_M$ SAD pattern in (*c*); and (*d*) $[001]_M$ SAD pattern.

The microstructures and diffraction patterns of samples aged at 538 °C were similar to those at 482 °C. In contrast, the precipitation progressed at a slightly faster rate, and the precipitates were slightly larger. A BF micrograph (Figure 8(a)) and a DF micrograph (Figure 8(b)) taken from the Ni_3Ti spot indicated by the arrow in the $[011]_M$ SAD pattern in Figure 8(c) reveal rod-shaped precipitates 12 nm in diameter and 60-nm long. Also, larger amounts of reverted austenite compared to those at 482 °C are present (Figures 8(a) and (b)).

The changes in the dimensions of the Ni_3Ti precipitates as a function of aging time at 482 °C and 538 °C were measured from DF micrographs taken from a Ni_3Ti spot. The results are shown in the log-log plot of the average precipitate diameter against aging time in Figure 9. The 90 pct confidence interval was about ±10 pct of the average diameter. It is evident that the precipitate growth behavior obeys a relationship of the type $d = kt^n$, where d represents the precipitate diameter, t the aging time, n the growth exponent, and k a constant related to the activation energy of the growth process. The exponent n (1/slope) is obtained as ~0.2 (*i.e.*, 1/5). The activation energy for precipitate growth in this temperature range, determined by plotting the log of the time required to attain a certain precipitate diameter against the reciprocal of the aging temperature (K), was constant independent

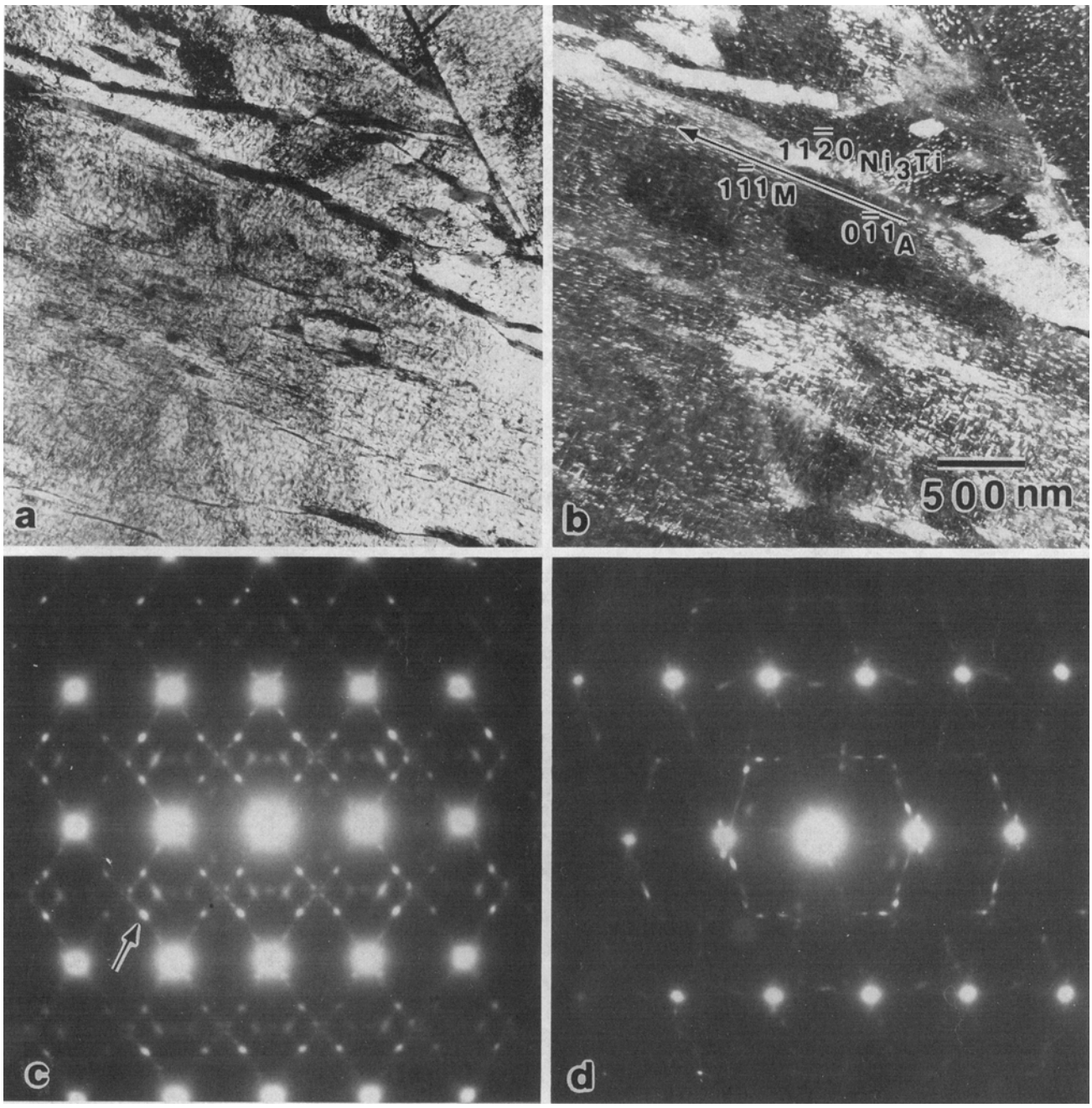

Fig. 8—T-250 steel aged at 538 °C for 50 h: (*a*) BF micrograph; (*b*) DF micrograph taken from the $(22\bar{4}0)$ Ni_3Ti spot indicated by the arrow in the $[011]_M$ SAD pattern in (*c*); and (*d*) $[113]_M$ SAD pattern.

of precipitate size with a value of 232 kJ/mole (56 kcal/mole), which is near the value for diffusion of Mo or Ti in α-Fe.[19]

2. *C-250 steel*

The behavior of this steel during the early stages of aging was largely similar to that of the T-grade. Streaking in diffraction patterns, appearance of weak precipitate spots, and nucleation of precipitates on dislocations and lath boundaries were observed. At 3 hours, the SAD patterns showed distinct precipitate spots, and DF micrographs revealed needle- or rod-shaped precipitates 5-nm wide and 22-nm long, slightly larger than those in the T-grade.[14] On the basis that the diffraction patterns in the initial stages (to 3 hours), in terms of positions of precipitate reflections and *d*-spacings, were identical to those obtained from the T-grade, it is concluded that the precipitating phase in the C-grade steel is also η-Ni_3Ti.

On continued aging to 50 hours, the Ni_3Ti precipitates coarsen considerably. A BF micrograph demonstrating this is shown in Figure 10(a). A $[011]_M$ SAD pattern (Figure 10(b)) shows besides Ni_3Ti spots, additional reflections having *d*-spacings which match those of the hexagonal Fe_2Mo with $a = 0.4745$ nm and $c = 0.7734$ nm.[20,21] This phase was also detected in the intermediate stages of aging—between 3 and 50 hours. The Ni_3Ti precipitates appear as rods 50 nm in diameter and 380-nm long, as shown in the DF micrograph in

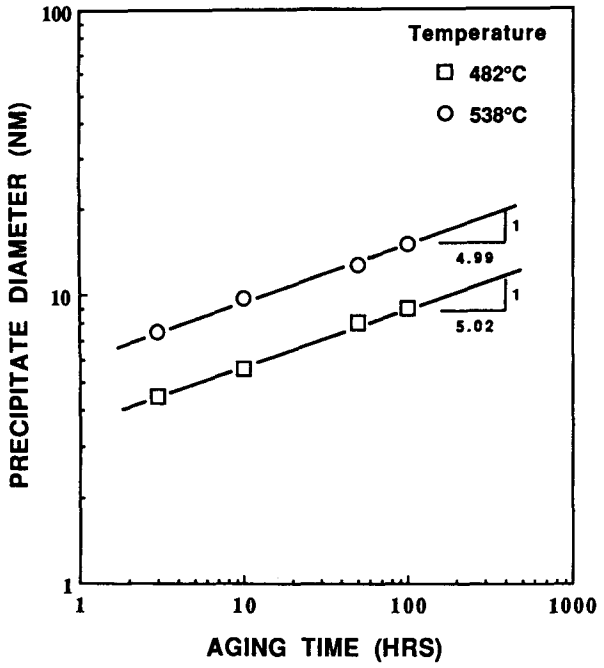

Fig. 9—Log-log plot of average precipitate diameter, d, against aging time, t, for T-250 steel aged at 482 °C and 538 °C.

Figure 10(c) taken from the $(\bar{2}\bar{2}40)$ spot labeled 1 in Figure 10(b); these dimensions are much larger than those of the precipitates in the T-grade. Besides these large precipitates, finer Ni_3Ti precipitates are also present. Since the {220} austenite spots coincide with the $\{22\bar{4}0\}$ spots of Ni_3Ti, it appears that some of the large particles in Figure 10(c) are reverted austenite; the latter was more frequently present as long, continuous, patchy regions on martensite lath boundaries in considerably larger amounts compared to the T-250 steel. Evidence for the presence of numerous spherical precipitates of Fe_2Mo of average size 20 nm is presented in the DF micrograph in Figure 10(d) taken from the spot labeled 2 in Figure 10(b).

The aging reactions at higher temperatures (538 °C) were similar to those at 482 °C. The reactions progressed somewhat faster, the resulting precipitates were coarser, and reverted austenite was detected earlier. The microstructure at 50 hours shows similar features, that is, coarse rods of Ni_3Ti (Figure 11(b)), spherical Fe_2Mo particles (Figure 11(c)), and long, patchy regions of reverted austenite (Figure 11(d)).

Energy-dispersive X-ray microanalysis of the precipitates in samples of both steels aged at 538 °C for 50 hours was carried out. The average composition, based on analysis of 15 particles in each case, together with the stoichiometric formulas, is given in Table IV. In the T-250 steel, the stoichiometric formula for the rod-shaped precipitates is obtained as $(Ni, Fe)_{3.6}(Ti, Mo)$. Evidently, some Fe substitutes for the Ni and some Mo for the Ti. In the case of the C-250 steel, a larger amount of Mo substitutes for the Ti in the Ni_3Ti precipitates. The stoichiometry obtained for these corresponds to $(Ni, Fe, Co)_{3.8}(Ti, Mo)$. This quantitative analysis is taken as confirmatory evidence for the formation of Ni_3Ti precipitates. The spherical precipitates in the C-250 steel are enriched with Fe and Mo; Ni and small amounts of Ti were also present. The stoichiometric formula corresponds to $(Fe, Ni, Co)_{2.2}(Mo, Ti)$, which is quite close to Fe_2Mo, assuming that Ni and Co substitute for the Fe and Ti substitutes for the Mo. Thus, in the C-grade, at peak strength, both Ni_3Ti and Fe_2Mo are present.

IV. DISCUSSION

A. *Identity of Maraging Precipitates*

The precipitation behavior and strengthening mechanisms in maraging steels have been extensively studied.[2–10] Although the general physical metallurgy of these steels is well understood, there is a diversity of opinion on the nature of the strengthening precipitates, particularly in the C-grade steels. For instance, in C-grade steels of similar composition, a variety of precipitates, such as Ni_3Mo,[2–5] Ni_3Ti,[4,5,6] Fe_2Mo,[6,7,8] FeTi,[2] and Fe_2Ti,[3] has been reported. Often more than one type of precipitate has been reported.[2–7] This diversity of precipitate identification has stemmed primarily from the close similarities in the structures and d-spacings of these various precipitates. Moreover, the identification is further complicated by the presence of more than one precipitate and by double diffraction effects. Changes in alloy chemistry and aging temperature also affect the nature of the precipitates.[1]

In the present study, it has been shown that the maraging precipitates in the C-250 steel are the hexagonal $(Ni, Fe)_3(Ti, Mo)$ and the hexagonal $(Fe, Ni, Co)_2(Mo, Ti)$, in agreement with the results of Miller and Mitchell;[6] the former are present initially, and the latter appear at intermediate aging times. The Ni_3Ti precipitates are not entirely replaced by the Fe_2Mo precipitates, as concluded by others.[6,7] In the T-250 steel, only $(Ni, Fe)_3(Ti, Mo)$ precipitates are present throughout the aging, confirming the findings of Vanderwalker.[9,10]

The identification of Ni_3Mo as the initial maraging precipitate by previous investigators[2–5] is not surprising in view of the close similarities between the structures and d-spacings of this compound and those of the hexagonal Ni_3Ti structure. The Ni_3Mo compound has an orthorhombic structure with $a = 0.5064$ nm, $b = 0.4224$ nm, and $c = 0.4448$ nm. However, if no attention is paid to the weak reflections due to ordering and if the slight orthorhombic distortion is neglected, its structure can be described as a reduced hexagonal cell with $a = 0.2532$ nm, $c = 0.4224$ nm, and $c/a = 1.67$.[22] The corresponding parameters for the hexagonal Ni_3Ti are $a = 0.5101$ nm, $c = 0.8307$, and $c/a = 1.63$.[15,16] It is clear that the c/a ratios of the two structures are quite close, and moreover, since the a and c parameters of Ni_3Ti are approximately twice that of the pseudo-hexagonal Ni_3Mo, equivalent reflections of the two structures have d-spacings closely related by a 2 : 1 ratio. For example, the (0004) ($d = 0.207$ nm) and $(22\bar{4}0)$ ($d = 0.128$ nm) reflections of Ni_3Ti can be alternately indexed as the (0002) ($d = 0.211$ nm) and $(11\bar{2}0)$ ($d = 0.1266$ nm) reflections, respectively, of Ni_3Mo. However, the measured interplanar spacings and angles and the simulated diffraction patterns give a superior match with the hexagonal Ni_3Ti.

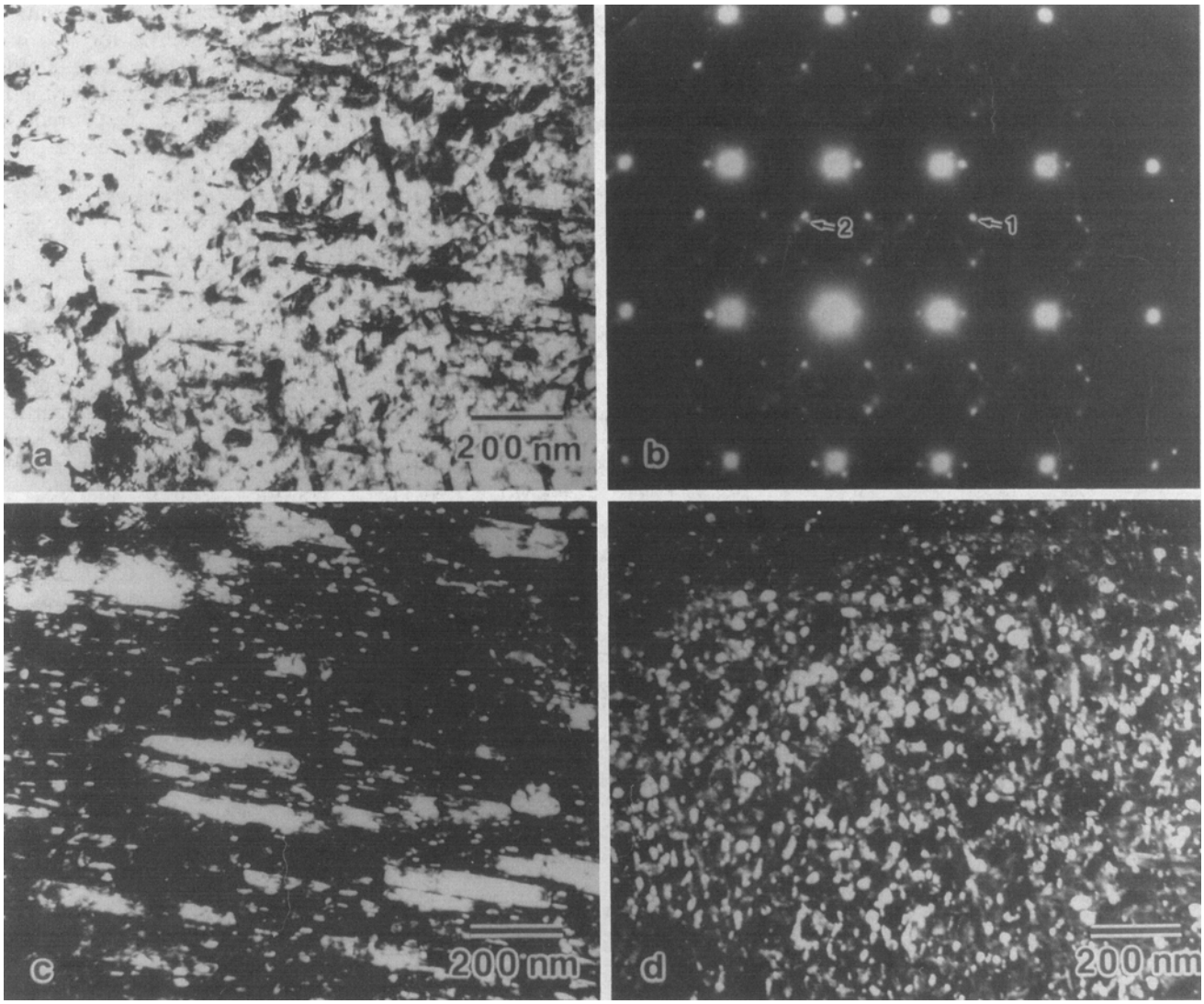

Fig. 10—C-250 steel aged at 482 °C for 50 h: (*a*) BF micrograph; (*b*) $[011]_M$ SAD pattern; (*c*) DF micrograph taken from the Ni_3Ti spot labeled 1 in (b); and (*d*) DF micrograph taken from the Fe_2Mo spot labeled 2 in (b).

The composition analyses give confirmatory evidence for the presence of $(Ni, Fe)_3(Ti, Mo)$ precipitates, with amounts of Ti significantly larger compared to Mo in the T-250 steel and being slightly lower in the C-250 steel. It has been pointed out that A_3B precipitates with a hexagonal close-packed (hcp) structure are favored because of the good lattice fit with the bcc martensite.[23,24] This is illustrated in Figure 12 by considering the atomic arrangement on the (011) martensite and (0001) Ni_3Ti planes. Based on the lattice parameters of these two structures, the lattice mismatch between the close-packed directions is obtained as 2.22 pct. An edge dislocation with $b = a/2\langle 111\rangle$ approximately every 25 atomic planes would accommodate this spacing difference. Thus, precipitates with lengths less than about 10 nm would be coherent with the martensite matrix, longer ones being semicoherent.

B. *Kinetics of Precipitation*

The interpretation of electrical resistivity data to derive kinetic information must be made with caution. The functional relationship between the resistivity and the degree of precipitation is a complicated and, quantitatively speaking, an unknown one. The complexity of the precipitation process, including the presence of coherency strains, more than one type of precipitate, and in the present case, the presence of reverted austenite, militates against a general analysis of the rates determined. In view of these considerations, the analysis must be regarded, at best, as a semiquantitative one.

There have been many previous studies showing that the isothermal aging kinetics of maraging steels could be expressed quite well by a relationship of the type $\Delta x/x_0 = kt^n$, where x is either electrical resistivity or hardness, x_0 is the solution-treated value, and k and n are constants.[25,26] Generally, n has a value between 0.2 and 0.4, well below the ideal value of 0.5 for the case of diffusion-controlled growth of platelets.[27] The activation energies are also low, in the range of 126 to 168 kJ/mole (30 to 40 kcal/mole), well below the typical values of 239 and 273 kJ/mole (57 and 65 kcal/mole) for diffusion of Mo and Ti, respectively, in α-Fe.[19]

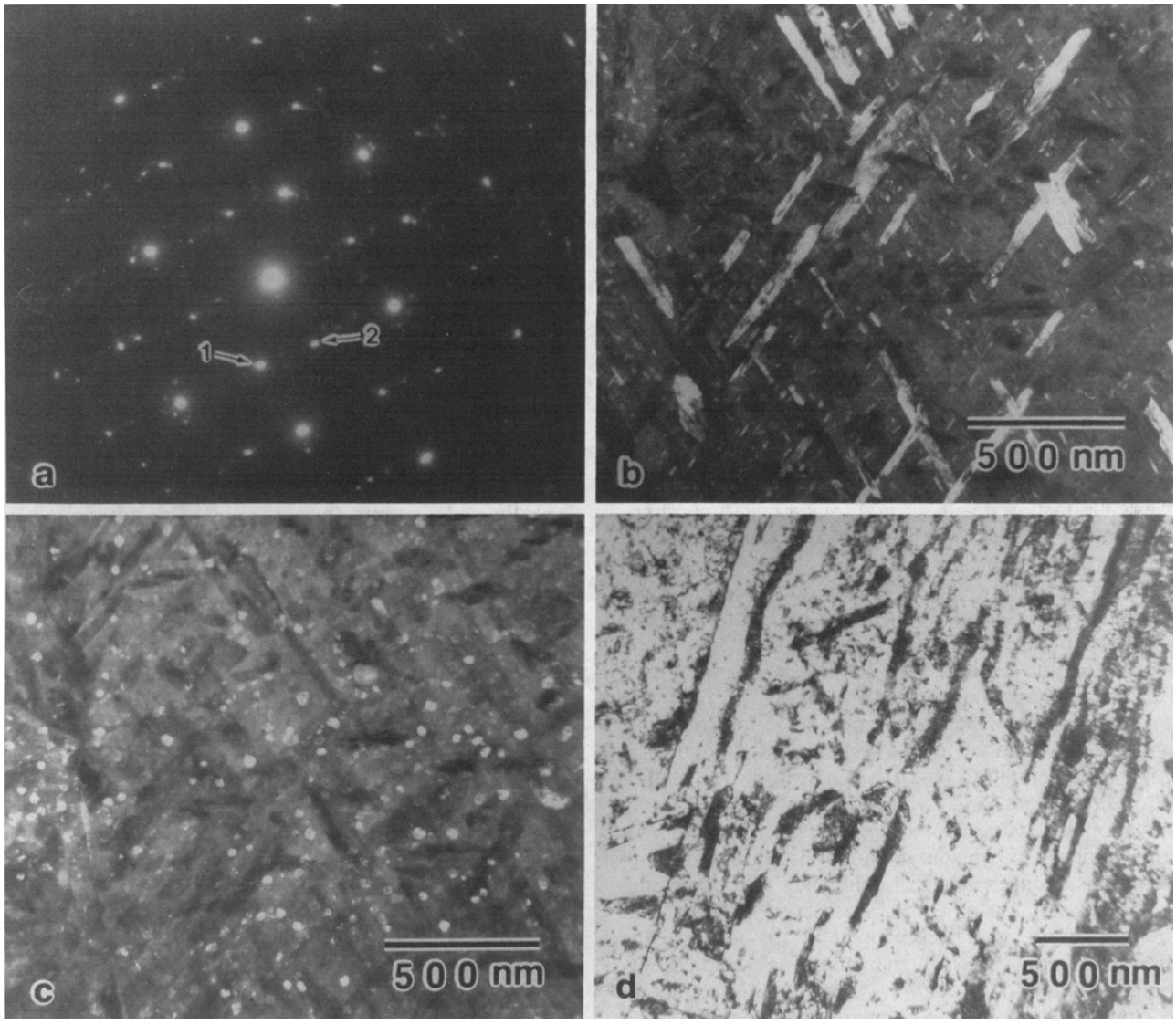

Fig. 11—C-250 steel aged at 538 °C for 50 h: (*a*) $[012]_M$ SAD pattern; (*b*) DF micrograph taken from the $(20\bar{2}1)$ Ni_3Ti spot labeled 1 in (a); (*c*) DF micrograph taken from the $(\bar{2}11\bar{1})$ Fe_2Mo spot labeled 2 in (a); and (*d*) BF micrograph showing long, patchy regions of reverted austenite at martensite lath boundaries.

The present results of electrical resistivity indicate that the precipitation kinetics can be described adequately by the Johnson-Mehl-Avarami equation. The values of the Avarami exponent n obtained varied with temperature in the C-250 steel, being 0.39, 0.39, and 0.45 at 427 °C, 482 °C, and 538 °C, respectively. These values are comparable to that reported by Peters and Cupp,[12] who assumed that the resistivity was proportional to the concentration of Mo and utilized a relationship of the type $\bar{C} = C_0 - kt^n$, where $\bar{C}$ is the average concentration, C_0 is the initial concentration, and k and n are constants. In the T-250 steel, a considerably lower but approximately constant n value of 0.20 is obtained.

The low values of n and the activation energy have

Table IV. Chemical Compositions of Precipitates

	T-250 Steel $(Ni, Fe)_{3.6}(Ti, Mo)$		C-250 Steel $(Ni, Fe, Co)_{3.8}(Ti, Mo)$		C-250 Steel $(Fe, Ni, Co)_{2.2}(Mo, Ti)$	
	Wt Pct	At. Pct	Wt Pct	At. Pct	Wt Pct	At. Pct
Fe	10.5	10.9	13.3	14.6	49.3	59.9
Ni	68.3	67.5	59.7	62.4	5.8	6.7
Co	0.0	0.0	2.2	2.3	2.1	2.5
Mo	6.5	3.9	17.2	11.0	41.8	29.6
Ti	14.7	17.8	7.6	9.7	1.0	1.4

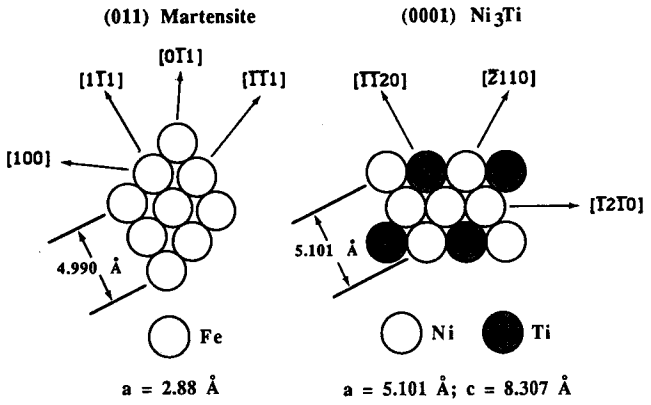

Fig. 12—Lattice matching of martensite and η-Ni_3Ti.

been commonly interpreted in terms of initial precipitation on dislocations, followed by growth on these dislocations by a pipe diffusion mechanism.[12] It has been suggested[12] that an n value near 1/3 is a one-dimensional manifestation of the Cottrell and Bilby[28] and Harper[29] law for precipitation on dislocations, which predicts an n value of 2/3. The subject of precipitation on dislocations has been treated theoretically by Cahn[30] for the case of a cylindrical, incoherent precipitate lying along a dislocation and having $\Delta G_{strain} = 0$. By assuming that the effect of nucleation on a dislocation is to provide further reductions in ΔG by the release of the strain energy of the dislocation, he showed that under conditions of high supersaturation, the free energy barrier for nucleation disappears, and nucleation on dislocations may occur spontaneously, *i.e.*, as rapidly as diffusion will permit. More sophisticated calculations, utilizing many assumptions about the state of coherency of the nucleus, have been made by others[31–34] to show that coherent nuclei may form in regions close to a dislocation, due to the interactions between the long-range strain fields of both nucleus and dislocation,[33] and that the reduction in the nucleation barrier is comparable for coherent and incoherent nuclei.[34]

These theoretical predictions are adequately satisfied in the steels studied, which together with experimental results, provide strong evidence for copious precipitation on dislocations, in agreement with other reports.[8,12] The electron diffraction evidence suggests that in the early stages of aging, coherent zones, presumably containing Ti and Mo, form on dislocations, from which Ni_3(Ti, Mo) precipitates develop. Garwood and Jones[35] have arrived at a similar conclusion based on electron microscopy studies of an Fe-25Ni-1.7Ti (wt pct) maraging steel. The observed variation in the activation energy determined from resistivity measurements from low values at short aging times to higher values at longer times, both values being lower than that for diffusion of either Ti or Mo in α-Fe, also suggests that the initial rate of nucleation is high and nuclei form on dislocations and subsequently grow by a pipe diffusion mechanism. Additional support is gathered from the observation that the electron microscopy studies give a $t^{1/5}$ dependence for precipitate growth, as predicted by theories on coarsening of precipitates on dislocations by a pipe diffusion mechanism.[36] However, the activation energy determined from these measurements is comparable to that for substitutional diffusion of Mo or Ti in α-Fe,[19] being somewhat higher than that determined by resistivity measurements. This difference may be reconciled on the basis that volume diffusion of solute to the precipitates from the matrix is contributory, and the dislocations serve as "collector lines" for solute from the matrix, along which precipitates subsequently coarsen by pipe diffusion, in a manner similar to that observed in Al-Zn alloys.[37] The variation in the activation energy during the course of aging, observed by resistivity measurements, is most probably related to the rate of nucleation, which decreases continuously with aging time. The higher values of the Avarami exponent, n, in the C-250 steel compared to the T-250 steel are clearly related to the additional precipitation of spherical Fe_2Mo precipitates in the former. A large fraction of these forms homogeneously in the martensite matrix (Figures 10 and 11), a process which is expected to raise the exponent n to higher values,[27] more so at the higher aging temperature (538 °C), where their formation proceeds rapidly and requires shorter times. The additional precipitation of this phase in the C-250 steel also accounts for the larger resistivity drop on aging compared to the T-250 steel.

Peters and Floreen[38] have argued that the precipitation kinetics, *i.e.*, the lack of an incubation time and low values of the activation energy, may not be dictated by the martensitic matrix and instead postulated that the close fit between A_3B compounds with the hcp structure and the bcc martensite was responsible. These conclusions were based on the observation of activation energies comparable to that of diffusion of substitutional elements in α-Fe in studies on the effect of prior cold work on the aging kinetics of an Fe-8Ni-13Mo steel which could be made ferritic or martensitic by appropriate heat treatment. Since this steel differs appreciably in composition from that of the C-250 and T-250 steels, it is quite likely that the precipitates which form are quite different. Moreover, precipitation on dislocations may not occur under conditions where the misfit vector of the precipitates and the Burgers vector of the matrix dislocations are nonparallel.[39] In view of these considerations, it is not possible to negate the influence of dislocations on the kinetics.

C. *Strengthening Behavior*

The hardening behavior of maraging steels is dependent on several factors. In the present study, it has been shown that the precipitate phases responsible for the strengthening of the C-250 steel are Ni_3Ti and Fe_2Mo, in agreement with Miller and Mitchell.[6] The Ni_3Ti precipitates are responsible for the initial hardening, whereas the peak strength and maintenance of high strength at longer times are caused by the presence of a fine distribution of Fe_2Mo precipitates. In the Co-free T-250 grade, only Ni_3Ti precipitates are observed. The higher Ti concentration results in a larger volume fraction of Ni_3Ti precipitates, which, in addition, are remarkably resistant to coarsening. The former is responsible for the high strength, comparable to that of the C-250 grade; the latter feature aids in maintaining high strength at longer aging times. Another contribution to the strength possibly comes from ordering of the matrix. It is likely that

some B2-type ordering of FeNi and/or FeCo (in C-250) occurs,[40] but this could not be established positively, because the positions of diffraction indicating B2 ordering also coincide with those expected for surface Fe_3O_4.[17,18]

Several investigators[4,41] have proposed that the strengthening can be accounted for by an Orowan relationship, namely,

$$\sigma_y = \sigma_0 + T/\mathbf{b}\Lambda \quad [4]$$

where σ_y is the total yield strength, σ_0 is the matrix yield strength, T is the line tension, $\mathbf{b}$ is the Burgers vector, and Λ is the interparticle spacing. Detert[24] utilized the expression put forth by Ansell and Lenel[42,43] to argue that a significant contribution to the strength comes from the high shear strength of the precipitates. However, he appears to have ignored the matrix strength, which if taken into account, would predict a yield strength considerably higher than observed. An attempt was made in the present study to predict the strengthening mechanism. The yield strength of the T-250 steel following aging at 482 °C for 6 hours is 250,000 psi (1723 MPa).[44] At this time, the present study shows that the precipitates are approximately 5.2 nm in diameter and 28-nm long. For the sake of simplicity, the rod shape can be replaced by a sphere of equivalent volume of diameter d = 10 nm. Taking the volume fraction of precipitates, f, as 5 pct,[24] the interparticle spacing, Λ, is obtained as 22.5 nm using the expression $(0.82d/\Lambda) = f^{1/3}$.[39] Utilizing a specific form of the Orowan relationship given by

$$\sigma_y = \sigma_0 + 2\,G\,\mathbf{b}\,\phi \ln(\Lambda - d/2\mathbf{b})/4\pi(\Lambda - d) \quad [5]$$

where G is the shear modulus of the matrix, ϕ is related to the Poisson's ratio of the matrix by $\phi = (1 + 1/1 - \nu)/2$, and other variables have the same meanings as before. Taking G = 71 GPa (10.3 million psi), $\nu = 0.3$,[45] and σ_0 = 95,000 psi (655 MPa),[44] a yield strength of 223,000 psi (1540 MPa) is obtained, in reasonable agreement with the observed value.

The strengthening mechanisms in the T-250 steel can be summarized as follows. In the beginning stages of aging, strengthening is associated with the stress required for dislocations to cut through coherent zones/precipitates of Ni_3Ti. The work done in forcing the dislocations through the precipitates may be governed by coherency stresses and internal ordering of the precipitates. As the precipitates coarsen and become semicoherent, the stress required for dislocations to cut through them increases, so that the yield strength increases. Eventually, the precipitates grow to an extent that dislocations are forced between them instead of through them, and peak strength results at a critical interparticle spacing. Further increase in particle size and spacing at longer aging times then leads to a decrease in strength, the yield strength being governed by the Orowan relationship, that is, varying as $1/\Lambda$.

Loss of strength is associated more importantly with reversion to austenite. The effect of alloying elements on the tendency to austenite reversion is well known.[46] The rate of formation and the volume fraction of reverted austenite increase with an increase in Ni and Mo contents and decrease with an increase in Co and Ti contents.[46] Thus, in the T-250 steel, the formation of Ni_3Ti results in depletion of Ni from the martensite matrix. For example, 1.4 wt pct Ti would tie up about 6 wt pct Ni, thereby reducing the Ni content in the martensite matrix to about 12 wt pct and the volume fraction of reverted austenite, as confirmed by the microstructural observations.

In the case of the C-250 grade, the effects are more subtle because of the influence of Co. The effect of cobalt, although long recognized as an important alloying addition, has remained unclear. Miller and Mitchell[6] attributed the effect of Co to a combination of matrix hardening and reduction in the solubility of Mo, which results in a finer Fe_2Mo precipitate distribution. The latter effect was supported by Peters and Cupp,[12] who based on electrical resistivity and hardness measurements, suggested that the effect of cobalt is to raise the supersaturation of Mo, thereby resulting in a finer distribution of Mo-rich intermetallics. On the other hand, the precipitation of Fe_2Mo would result in depletion of Fe from the martensite matrix, thus raising the relative Ni content and the volume fraction of reverted austenite. Since Co increases the resistance to austenite reversion,[46] an additional effect is to partially mitigate the reverse tendency caused by the higher Mo content in the C-grade.

V. CONCLUSIONS

In conclusion, the nature of the strengthening precipitates in maraging steels C-250 and T-250 has been determined. The strengthening of the Co-free, higher Ti T-250 steel is caused by a refined distribution of Ni_3Ti precipitates; the maintenance of high strength at longer times results from the combined effect of a high resistance of these precipitates to coarsening and small volume fraction of reverted austenite. In the case of the Co-containing, lower Ti C-250 steel, strengthening results from the combined presence of Ni_3Ti (initially) and Fe_2Mo precipitates (at longer times). Loss of strength at longer times is associated, in part, with classical overaging and mainly from the larger volume fraction of reverted austenite.

ACKNOWLEDGMENTS

This work was supported by the United States Army Research Office under Contract No. DAAL-0386-K-0012. A portion of the electron microscopy was performed using the facilities at the Center for Microanalysis of Materials, operated by the Materials Research Laboratory at the University of Illinois.

REFERENCES

1. S. Floreen: *Met. Rev.*, 1968, vol. 13, pp. 115-28.
2. J.M. Chilton and C.J. Barton: *Trans. Q. ASM*, 1967, vol. 60, pp. 528-42.
3. B.G. Reisdorf: *Trans. Q. ASM*, 1963, vol. 56, pp. 783-86.
4. A.J. Baker and P.R. Swann: *Trans. Q. ASM*, 1964, vol. 57, pp. 1008-11.
5. K. Shimizu and H. Okamoto: *Trans. Jpn. Inst. Met.*, 1971, vol. 12, pp. 270-79.
6. G.P. Miller and W.I. Mitchell: *J. Iron Steel Inst.*, 1965, vol. 20, pp. 899-904.
7. H.L. Marcus, L.H. Schwartz, and M.E. Fine: *Trans. Q. ASM*, 1966, vol. 59, p. 468.

8. J.B. Lecomte, C. Servant, and G. Cizeron: *J. Mater. Sci.*, 1985, vol. 20, pp. 3339-52.
9. D.M. Vanderwalker: *Metall. Trans. A*, 1987, vol. 18A, pp. 1191-94.
10. D.M. Vanderwalker: in *Maraging Steels—Recent Developments and Applications*, TMS-AIME, Warrendale, PA, 1988, pp. 255-68.
11. G. Cliff and G.W. Lorimer, Jr.: *J. Microsc.*, 1975, vol. 103, pp. 203-07.
12. D.T. Peters and C.R. Cupp: *Trans. TMS-AIME*, 1966, vol. 236, pp. 1420-29.
13. J. Burke: in *The Kinetics of Phase Transformations in Metals*, Pergamon Press, New York, NY, 1965, pp. 36-60.
14. V.K. Vasudevan, S.J. Kim, and C.M. Wayman: in *Maraging Steels—Recent Developments and Applications*, TMS-AIME, Warrendale, PA, 1988, pp. 283-93.
15. A. Taylor and R.W. Floyd: *Acta Crystallogr.*, 1950, vol. 3, pp. 285-89.
16. P. Villars and L.D. Calvert: in *Pearson's Handbook of Crystallographic Data for Inter-metallic Phases*, ASM, Metals Park, OH, 1985, vol. 3, p. 2905.
17. A.T. Davenport: *J. Iron Steel Inst.*, 1968, vol. 206, pp. 499-501.
18. S.R. Keown and D.J. Dyson: *J. Iron Steel Inst.*, 1966, vol. 204, pp. 832-36.
19. M.A. Krishtal: in *Diffusion Processes in Iron Alloys*, translated from Russian by the Israel Program for Scientific Translations Ltd., Jerusalem, Israel, 1970, pp. 175-203.
20. C.J. Bechtoldt and H.C. Vacher: *J. Res. Nat. Bur. Stand. (U.S.)*, 1957, vol. 58, p. 7.
21. A.F. Yedneral and M.D. Perkas: *Fiz. Met. Metalloved.*, 1969, vol. 28, pp. 862-71.
22. S. Saito and P. Beck: *Trans. TMS-AIME*, 1959, vol. 215, pp. 938-41.
23. R.K. Pitler and G.S. Ansell: *Trans. Q. ASM*, 1964, vol. 56, pp. 220-46.
24. K. Detert: *Trans. Q. ASM*, 1966, vol. 59, pp. 262-76.
25. S. Floreen and R.F. Decker: *Trans. Q. ASM*, 1962, vol. 55, p. 518.
26. S. Floreen: *Trans. Q. ASM*, 1964, vol. 57, p. 38.
27. J.W. Christian: in *The Theory of Phase Transformations in Metals and Alloys*, Pergamon Press, New York, NY, 1965, pp. 471-95.
28. A.H. Cottrell and B.A. Bilby: *Proc. Phys. Soc.*, 1949, vol. A62, p. 49.
29. S. Harper: *Phys. Rev.*, 1951, vol. 83, p. 209.
30. J.W. Cahn: *Acta Metall.*, 1957, vol. 5, p. 169.
31. C.C. Dollins: *Acta Metall.*, 1970, vol. 18, p. 1209.
32. R. Gomez-Ramirez and G.M. Pound: *Metall. Trans.*, 1973, vol. 4, pp. 1563-70.
33. L. Katgerman and J. Van Liere: *Acta Metall.*, 1978, vol. 26, pp. 361-67.
34. K.C. Russell and H.I. Aaronson: *J. Mater. Sci.*, 1975, vol. 10, pp. 1991-99.
35. R.D. Garwood and R.D. Jones: *J. Iron Steel Inst.*, 1966, vol. 204, pp. 512-19.
36. H. Kreye: *Z. Metallkd.*, 1970, vol. 61, pp. 108-12.
37. R.M. Allen and J.B. Vander Sande: in *Solid → Solid Phase Transformations*, H.I. Aaronson, D.E. Laughlin, R.F. Sekerka, and C.M. Wayman, eds., TMS-AIME, Warrendale, PA, 1982, pp. 655-59.
38. D.T. Peters and S. Floreen: *Trans. AIME*, 1969, vol. 245, pp. 2021-26.
39. A. Kelly and R.B. Nicholson: *Prog. Mater. Sci.*, 1963, vol. 10, pp. 149-391.
40. Stephen Spooner, H.J. Rack, and David Kalish: *Metall. Trans.*, 1971, vol. 2, pp. 2306-08.
41. B.G. Reisdorf and A.J. Baker: *Air Force Materials Laboratory Tech. Rep.*, Wright-Patterson Air Force Base, Dayton, OH, 1965, no. AFML-TR-64-390.
42. G.S. Ansell and F.V. Lenel: *Acta Metall.*, 1960, vol. 8, pp. 612-16.
43. G.S. Ansell: *Acta Metall.*, 1961, vol. 9, pp. 518-19.
44. S. Floreen and A.M. Bayer: in *Maraging Steels—Recent Developments and Applications*, TMS-AIME, Warrendale, PA, 1988, pp. 39-54.
45. R.F. Decker: in *Source Book on Maraging Steels*, ASM, Metals Park, OH, 1979, p. 358.
46. D.T. Peters: *Trans. Q. ASM*, 1968, vol. 61, pp. 62-67.